Arsenic-bearing new mineral species from Valletta mine, Maira Valley, Piedmont, Italy: I. Grandaite, Sr2Al(AsO4)2(OH), description and crystal structure

Revision 1

As-bearing new mineral species from Valletta mine, Maira Valley, Piedmont, Italy: I. Grandaite, $Sr_2Al(AsO_4)_2(OH)$, description and crystal structure

F. CÁMARA[1,2]*, M.E. CIRIOTTI[3], E. BITTARELLO[1,2], F. NESTOLA[4], F. MASSIMI[5], F. RADICA[6], E. COSTA[1], P. BENNA[1,2] AND G.C. PICCOLI[7]

[1]Dipartimento di Scienze della Terra, Università degli Studi di Torino, via Tommaso Valperga Caluso 35, I-10125 Torino, Italy

[2]CrisDi, Interdepartmental Centre for the Research and Development of Crystallography, via Pietro Giuria 5, I-10125, Torino, Italy

[3]Associazione Micromineralogica Italiana, via San Pietro 55, I-10073 Devesi-Cirié, Torino, Italy

[4]Dipartimento di Geoscienze, Università degli Studi di Padova, via G. Gradenigo 6, I-35131 Padova, Italy

[5]Dipartimento di Ingegneria Meccanica e Industriale, Università degli Studi Roma Tre, via della Vasca Navale 79, I-00146 Roma, Italy

[6]Dipartimento di Scienze Geologiche, Università degli Studi Roma Tre, largo San Leonardo Murialdo 1, I-00146 Roma, Italy

[7]Amici del Museo "F. Eusebio", via Paruzza 1, I-12051 Alba, Italy

*correspondent author's e-mail: fernando.camaraartigas@unito.it

ABSTRACT

The new mineral species grandaite, ideally $Sr_2Al(AsO_4)_2(OH)$, has been discovered on the dump of Valletta mine, Maira Valley, Cuneo province, Piedmont, Italy. Its origin is related to the reaction between the ore minerals and hydrothermal solutions. It occurs in thin masses of bright orange to salmon to brown colour, or infrequently as fan-like aggregates of small (< 1 mm) crystals, with reddish brown streak and waxy to vitreous lustre. Grandaite is associated with aegirine, baryte, braunite, hematite, tilasite, quartz, unidentified Mn-oxides, and Mn-silicates under study.

Grandaite is biaxial positive with refractive indices $\alpha = 1.726(1)$, $\beta = 1.731(1)$, $\gamma = 1.752(1)$. Its calculated density is 4.378 g/cm^3. Grandaite is monoclinic, space group $P2_1/m$, with a 7.5764(5), b 5.9507(4), c 8.8050(6) Å, β 112.551(2)°, V 366.62(4) Å^3 and Z 2. The eight strongest diffraction lines of the observed X-ray powder diffraction pattern are [d in Å, (I), (hkl)]: 3.194 (100)(-211), 2.981 (50.9)(020), 2.922 (40.2)(-103), 2.743 (31.4)(120), 2.705 (65.2)(112) , 2.087 (51.8) (-123), 1.685 (24.5)(321), 1.663 (27.7)(132). Chemical analyses by electron microprobe gave (wt.%) SrO 29.81, CaO 7.28, BaO 1.56, Al_2O_3 7.07, Fe_2O_3 2.34, Mn_2O_3 1.88, MgO 1.04, PbO 0.43, As_2O_5 44.95, V_2O_5 0.50, P_2O_5 0.09, sum 96.95; H_2O 1.83 wt.% was calculated by stoichiometry from the results of the crystal structure analysis. Raman and infrared spectroscopies confirmed the presence of $(AsO_4)^{3-}$ and OH groups. The empirical formula calculated on the basis of 9 O a.p.f.u., in agreement with the structural results, is $(Sr_{1.41}Ca_{0.64}Ba_{0.05}Pb_{0.01})_{\Sigma=2.11}(Al_{0.68}Fe^{3+}_{0.14}Mn^{3+}_{0.12}Mg_{0.13})_{\Sigma=1.07}[(As_{0.96}V_{0.01})_{\Sigma=0.97}O_4]_2(OH)$, the simplified formula is $(Sr,Ca)_2(Al,Fe^{3+})(AsO_4)_2(OH)$ and the ideal formula is $Sr_2Al(AsO_4)_2(OH)$.

The crystal structure was solved by direct methods and found to be topologically identical to that of arsenbrackebuschite. The structure model was refined on the basis of 1442 observed reflections to R_1 2.78%. In the structure of grandaite, chains of edge-sharing M^{3+}–octahedra run along [010] and share vertices with T^{5+} tetrahedra, building up $[M^{3+}(T^{5+}O_4)_2(OH, H_2O)]$ units,

which are connected through interstitial divalent cations. Grandaite is named after the informal appellation of the province in which the type locality is located. The new mineral was approved by IMA CNMNC (2013-059). The discovery of grandaite and of other members of the group (description still in progress) opens up the possibility of exploring the crystal chemistry of the brackebuschite supergroup.

Keywords: grandaite, arsenate, arsenbrackebuschite-group, new mineral species, crystal structure, Valletta, Piedmont, Italy

INTRODUCTION

Arsenic is not a very abundant element. It accounts for about 1.5 ppm of the Earth's crust, making it the 47th most abundant element (Vaughan, 2006). On average, soils contain 1–10 ppm of arsenic, while seawater has only 1.6 ppb As (Emsley, 2011). In its more common natural form, arsenic occurs as colourless, odourless, crystalline As_2O_3 (the lethal "white arsenic" corresponding to both arsenolite and claudetite) and As_2O_5, which are hygroscopic and readily soluble in water to form acidic solutions. Arsenic acid (containing As^{5+}), $AsO(OH)_3$, is a weak acid, which forms arsenates responsible for arsenic contamination of groundwater, a problem that affects many people (*e.g.* Mukherjee *et al.*, 2006; Twarakavi and Kaluarachchi, 2006), making the geochemical investigation of arsenic very important.

In some respects arsenic compounds resemble those of phosphorus (another Group V element). The protonation steps between the arsenate and arsenic acid are similar to those between phosphate and phosphoric acid. The most common oxidation states for arsenic are: -3 in the arsenides (such as alloy-like intermetallic compounds), and +3 in the arsenites, +5 in the arsenates, and most organoarsenic compounds. Arsenic also bonds readily to itself as seen for example in the square As^{-3}_4 ions in the mineral skutterudite. In oxides, As^{+3} typically occurs as a pyramidal AsO_3 group in which all oxygens lie to one side of the As^{+3} ion due to a stereoactive lone pair of electrons (Norman, 1998), while in the +5 oxidation state it is typically tetrahedrally coordinated.

To date more than 260 arsenates and fewer than 30 arsenites and less than 10 silicoarsenates are recognized as valid mineral species by IMA CNMNC. The recognition of new arsenate mineral species at the Valletta mine dumps (Piedmont, Italy) make this a significant mineralogical locality. Grandaite (IMA-CNMNC no. 2013–059) represents the third Sr–dominant arsenate between the mineral species recognized as valid by IMA CNMNC, after arsenogoyazite, $SrAl_3(AsO_4)(AsO_3OH)(OH)_6$ (Walenta and Dunn, 1984), and kemmlitzite, $SrAl_3(AsO_4)(SO_4)(OH)_6$

(Hak *et al.*, 1969). The new mineral species strontiopharmacosiderite, $Sr_{0.5}Fe^{3+}_4(AsO_4)_3(OH)_4 \cdot 4H_2O$ (S. J. Mills, pers. com. 2013) was approved afterwards (IMA–CNMNC 2013–101).

This is the first of a series of formal descriptions of new As–bearing minerals from the Valletta mine. Sample containing grandaite was collected by one of the authors (GCP) in 2001 and later in 2009 on the dumps of the Valletta mine, Valletta Valley ("Vallone della Valletta" in Italian), Canosio municipality, Maira Valley, Cuneo province, Piedmont, Italy (44°23'542" N, 7°5'42" E, 2536 m asl). The Valletta mine is a small Fe–Mn–As deposit that has never been studied geologically or petrologically. The name of grandaite is for the informal appellation of the Province in which the type locality (Valletta mine) is located. The Cuneo Province is popularly and historically called "la Granda" (the Big One) for its considerable extent, mostly in the Alpine region (Maritime and Cottian Alps south of Mount Monviso). At 6903 km² it is one of the biggest in Italy.

A fragment of holotype material is deposited in the mineralogical collection of the Museo Regionale di Scienze Naturali di Torino, Sezione di Mineralogia, Petrografia e Geologia, via Giovanni Giolitti 36, I–10123 Torino, Italy, catalogue number M/15999, and another in the mineralogical collection of the Museo Civico Archeologico e di Scienze Naturali "Federico Eusebio", via Vittorio Emanuele 19, I–12051 Alba, Cuneo, Italy, catalogue number G. 1723 prog. 505.

Not long after submitting the manuscript our good friend and colleague Bruno Lombardo passed away. He very much loved the Alps and has devoted much effort to the Piedmont mineralogy contributing passionately to the exploration and knowledge of many mineralogical localities. We wish to dedicate this paper to his memory.

GEOLOGICAL SETTING AND MINERAL OCCURRENCE

The Valletta Fe-Mn deposit is located in the Briançonnais Zone of the Cottian Alps. Specifically, the Mn minerals are hosted in Permian quartzites overlying quartzose conglomerates of the Verrucano facies and quartz-feldspar fine-grained schists deriving from Permian rhyolitic

112 volcanism of the so-called Axial Permian-Carboniferous Zone (Franchi and Stella, 1930). A major
113 subvertical tectonic contact, Faille de Ceillac (Gidon *et al.*, 1994) separates the rocks found at
114 Valletta mine to the north from the Middle Triassic carbonate sequence of the Becco Grande -
115 Rocca La Meia ridge to the south. The rocks found at Valletta mine are part of the Bande de
116 Marinet, the southernmost tectonic zone of the Axial Permian-Carboniferous Zone; specifically it is
117 part of Unit M3, the structurally highest unit defined in the Bande de Marinet by Lefèvre (1982).
118 During the Alpine tectonometamorphic cycle the rocks now exposed in the Bande de Marinet were
119 subjected to High-*P*, Low-*T* metamorphism of blueschist facies, whose effects are more evident in
120 the metabasites intercalated in the metavolcanic quartz-feldspar schists that often display the
121 characteristic lawsonite-glaucophane assemblage (Franchi and Stella, 1930; Gidon *et al*., 1994).
122 Probably grandaite is the result of the crystallization from hydrothermal fluids in a relatively
123 oxidizing environment (the occurrence of hematite, braunite, arsenates agree with this hypothesis);
124 As can be likely derived from the surrounding Fe-Mn ores, as observed by several authors in other
125 small hydrothermal Fe-Mn deposits from Alps (e.g., Brugger and Gieré, 1999).

126 A brief mineralogical note on the Valletta mine was given by Piccoli (2002). At a first
127 exploration, the remains of an old mining operation, probably an open pit, were found at the head of
128 the Valletta Valley, near Canosio, in the Maira Valley (Cuneo, Piedmont, Italy). Historical
129 information on a mine active in 1455 in the Saluzzo Marquisate (of which Canosio was part) are
130 summarized by Mangione (1999) and Pipino (2010). The translation of the historical medieval text
131 is as follows: "*September 10, 1455: Perpetual lease made by the Marquis Ludovico di Saluzzo to*
132 *Antonio Petro, late Petrino, and Antonio Bordello, alias Poncetto, of a small assay of an iron mine*
133 *in the territory of Canosio, at the Valletta, with 12 fathoms of land not so far, by the tithe of the*
134 *ore*."

135 However, the deposit has never been studied from a genetic point of view and available
136 geological data for the studied area are very limited. Other than the historic text above reported,
137 there is no mention in the literature of the occurrence of ore mineralizations. Preliminary work

carried out during sampling of grandaite showed that it is a small Fe-(Mn) deposit enriched in arsenic. Grandaite-bearing quartz veins are hosted within compact, granular, dark red (verging on black) quartzite. Blocks of this material have been dug and piled up in a small landfill where they are mixed with calcareous rocks also from the excavated material.

The new mineral is strictly associated with aegirine, adelite $CaMg(AsO_4)(OH)$, baryte, braunite, hematite, quartz, tilasite $CaMg(AsO_4)F$, unidentified Mn oxides, and Mn silicates under study.

In addition to grandaite a number of other As-rich mineral species occurs in this small dump, some of them are currently under study. This findings make the small dump of the Valletta mine a reference locality for the study of arsenates and silicoarsenates mineral species, similar to those of the Graveglia Valley, Liguria, Italy (Antofilli *et al*., 1983; Borgo and Palenzona, 1988; Palenzona, 1991, 1996). Other As-rich minerals found in the rock samples collected in the dump, although not strictly associated with grandaite are: arseniopleite–caryinite series $(Ca,Na)NaMn^{2+}(Mn^{2+},Mg,Fe^{2+})_2(AsO_4)_3$ – $(Na,Pb)(Ca,Na)CaMn^{2+}{}_2(AsO_4)_3$, azurite, berzeliite $NaCa_2Mg_2(AsO_4)_3$, manganberzeliite $NaCa_2Mn^{2+}{}_2(AsO_4)_3$, tiragalloite $Mn^{2+}{}_4As^{5+}Si_3O_{12}(OH)$, braccoite (IMA 2013-093) $NaMn^{2+}{}_5[Si_5As^{5+}O_{17}(OH)](OH)$; these are found along with albite, calcite, diopside, ganophyllite, ilmenite, hollandite, malachite, magnesio–riebeckite, magnetite, Mn–bearing muscovite, orthoclase, rutile, rhodonite and titanite.

MINERALOGICAL CHARACTERIZATION

Appearance and physical properties

Grandaite occurs as subhedral crystals in thin masses, a few cm in size, with uneven fracture (Fig. 1), or infrequently as fan-like aggregates of small crystals, in white veins of compact quartz on reddish-brownish-black K-feldspar crossing, in a disorganized manner, the granular red-brown

quartzite. Well-formed crystals, typically platy tablets, are very rare and are rarely included in more hyaline quartz and/or blackish matrix on fracture surfaces.

Individual crystals are bright orange to salmon to brown, and no twinning is observed. Grandaite is translucent and has a reddish-brown streak, a waxy to vitreous lustre, and does not fluoresce under SW or LW ultraviolet light. Grandaite is optically biaxial positive, with a $2V$ (meas.) = 52(2)º and $2V$ (calc.) = 53º. The measured refractive indices are α = 1.726(1), β = 1.731(1), γ = 1.752(1) (589 nm).

The mineral is brittle. No cleavage or parting is observed. Hardness was measured by nano–indentation by using an Agilent Nano Indenter G200 at the Università di Roma Tre – LIME labs. performed in CSM (continuous stiffness measurement) mode, with a frequency of 45 Hz, amplitude of oscillation 2 nm, constant strain rate of 0.05 s^{-1}, and a maximum penetration depth 1000 nm. Results of hardness and modulus profiles were obtained after averaging over 25 different tests. The instrument was completely re-calibrated before testing by performing a series of indentations on a certified amorphous silica reference sample. Observed elastic modulus is 121.9 ± 11 GPa (displacement 90-110 nm) and hardness is H: 9.95 ± 1.29 GPa (displacement 90-110 nm); Vickers Hardness was calculated from H in order to calculate Mohs hardness, obtaining Mohs hardness of 6-6½. Because the method for obtaining hardness used a continuous variation of the load, it is not easy to provide actual Vickers hardness units. Density was not measured due to the small crystal size and its intergrowths with adelite and baryte. The calculated density obtained from the empirical formula and unit-cell parameters measured during the single-crystal study is 4.378 g/cm^3.

Chemical data

The chemical composition of grandaite was determined using a Cameca SX–50 electron microprobe (WDS mode) at the Dipartimento di Geoscienze (Università di Padova) on a thin section obtained from the holotype close to the place where the crystal used for the diffraction study was extracted. Major and minor elements were determined at 20 kV accelerating voltage and 20 nA

beam current (beam size 2 μm), with 40 to 20 s counting time on both peak and background. X–ray counts were converted to oxide wt.% using the PAP correction program supplied by Cameca (Pouchou and Pichoir, 1984, 1985).

The crystals studied in the thin section (Fig. 2) were found to be homogeneous. On the basis of previous quantitative SEM-EDS using a Cambridge S–360 microscope equipped with an Oxford INCA Energy 200 (with ultrathin window) at the Dipartimento di Scienze della Terra (Università di Torino), analyses Na, K, Y, REE, F and Cl were not sought in the WDS study; Si, Nb, Ti, Ta and S were checked but were below detection limits. The results of 8 analyses are given in Table 1.

The empirical formula, calculated on the basis of 9 O a.p.f.u., is, within rounding errors, $(Sr_{1.41}Ca_{0.64}Ba_{0.05}Pb_{0.01})_{\Sigma=2.11}(Al_{0.68}Fe^{3+}_{0.14}Mn^{3+}_{0.12}Mg_{0.13})_{\Sigma=1.07}[(As_{0.96}V_{0.01})_{\Sigma=0.97}O_4]_2(OH)$. The presence of OH was confirmed by Raman and FTIR (see next sections). Fe was considered as Fe^{3+} on the basis of site bond length observed from structure refinement. The simplified formula is $Sr_2Al(AsO_4)_2(OH)$, which requires SrO 41.68, Al_2O_3 10.23, As_2O_5 46.28, H_2O 1.81, total 100.00 wt.%. The mean refractive index *n* of grandaite, the calculated density and the empirical formula yielded a Gladstone-Dale compatibility index (Mandarino, 1979, 1981) of 0.032 rated as excellent.

Grandaite is unreactive and insoluble in 2 *M* and 10% HCl, and 65% HNO_3.

Micro-Raman spectroscopy

The Raman spectrum of grandaite (Fig. 3) was obtained at the Dipartimento di Scienze della Terra (Università di Torino) using a micro/macro Jobin Yvon Mod. LabRam HRVIS, equipped with a motorized *x*-*y* stage and an Olympus microscope. The backscattered Raman signal was collected with 50× objective and the Raman spectrum was obtained for a non-oriented crystal. The 632.8 nm line of an He-Ne laser was used as excitation; laser power was controlled by means of a series of density filters. The minimum lateral and depth resolution was set to few μm. The system was calibrated using the 520.6 cm^{-1} Raman band of silicon before each experimental session. The spectra were collected with 2–6 acquisitions, counting times ranging between 20 and 180 seconds.

Spectral manipulation such as baseline adjustment, smoothing and normalization were performed using the LabSpec 5 software package (Horiba Jobin Yvon GmbH, 2004, 2005) . Band component analysis was undertaken using the Fityk software package (Wojdyr, 2010), which enabled the type of fitting function to be selected and allows specific parameters to be fixed or varied accordingly. The spectrum was recorded using the LabSpec 5 program from 100 to 4000 cm^{-1} and the results of the spectroscopic analysis are reported below.

Bands with frequencies between 200 and 600 cm^{-1} correspond to As^{5+}–O bending vibrations, while bands lower than 200 cm^{-1} correspond to lattice modes (120, 162, 213 cm^{-1}).

In detail multiple Raman bands are observed at 308, 347, 382, 386, 418, 425 cm^{-1}. The first two bands are assigned to the v_2 $(AsO_4)^{3-}$ symmetric bending vibration (E) and the latter four bands are assigned to the v_4 bending vibration (F2). The assignment of these bands is in harmony with the analysis of arsenate vibrations according to Myneni *et al*. (1998a,b) and Nakamoto (1986). A broad band centered upon 500 cm^{-1}, which may be resolved into component bands at 499, 512, 526 and 547 cm^{-1} probably includes bands attributable to the v_4 $(AsO_4)^{3-}$ bending mode. The observation of multiple bands is characteristic of reduced symmetry of the AsO_4 unit in the crystal (Frost *et al*., 2011). In the range 700-950 cm^{-1} the spectra are complex, showing multiple bands that can be attributed to As^{5+}–O stretching vibrations of AsO_4^{3-} groups. A broad envelope of overlapping bands centered upon 858 cm^{-1}. Band component analysis enables bands to be resolved with two intense bands at 857 and 833 cm^{-1} observed. These bands are assigned to the v_1 $(AsO_4)^{3-}$ symmetric stretching and v_3 $(AsO_4)^{3-}$ antisymmetric stretching modes. Other bands are found at 899 and 790 cm^{-1} which may also be ascribed to the v_3 $(AsO_4)^{3-}$ antisymmetric stretching mode or may be attributed to the hydroxyl deformation mode (Frost *et al*., 2011). The absence of strong bands with frequencies higher than 950 cm^{-1} indicates the absence of H–, C–, N– and B-bearing groups in grandaite, but in the region between 2500 and 4000 cm^{-1} (hydroxyl stretching region) the spectrum displays a considerable amount of noise and this is a result of the low intensity of the bands. So the

presence of some measurable OH content is not excluded and for this reason we decided to collect the infrared spectrum of grandaite.

Infrared spectroscopy

IR spectra (Fig. 4) were collected at the Università di Roma Tre using a Bruker Hyperion 3000 IR-microscope equipped with liquid nitrogen-cooled MCT detector. The powder spectrum was collected with a Bruker Optics VERTEX 70v FTIR spectrometer equipped with a KBr beamsplitter, a DTGS detector and a MIRacle Diamond ATR accessory. For both, the nominal resolution was 4 cm^{-1} and 128 scans were averaged for background and sample. IR confirmed the presence of hydrogen (absorption band at ~3300 cm^{-1}) as hydroxyl showing strong hydrogen bonding. Using the Libowitzky (1999) correlation a frequency of 3200 cm^{-1} yields d(O···O) = 2.70 Å and d(H···O) = 1.85 Å. The presence of an absorption band at ~ 4100 cm^{-1} in the μ-IR spectrum can be assigned to combination of stretching and bending modes of (OH) groups, although they could be also assigned to hypertones or combinations related to the $(AsO_4)^{3-}$ group.

X–ray diffraction

The powder X–ray diffraction pattern of grandaite was obtained at CrisDi (Università di Torino) using an Oxford Gemini R Ultra diffractometer equipped with a CCD area detector, with graphite-monochromatised Mo$K\alpha$ radiation. Indexing of the reflections was based on a calculated powder pattern obtained by the structural model, using the software PLATON v–140513 (Spek, 2009). Experimental and calculated data are reported in Table 2.

The unit–cell parameters refined from the powder data with the software GSAS (Larson and Von Dreele, 1994) are a 7.575(1), b 5.9526(9), c 8.765(2) Å, β 112.55(2)° and V 366.62(4) $Å^3$.

Single-crystal X–ray diffraction data were collected using a Bruker AXS APEX SMART APEX diffractometer with a CCD detector (Mo$K\alpha$ radiation) at Università di Pavia (Pavia, Italy). A crystal fragment showing sharp optical extinction behaviour was used for collecting intensity data.

Crystal data and experimental details are reported in Table 3. The intensities of 6095 reflections with $-12 < h < 12$, $-9 < k < 9$, $-14 < l < 14$ were collected up to 69.9° 2θ using 0.2° frame and an integration time of 10 s. Data were integrated and corrected for Lorentz and polarization background effects, using the package SAINT V6.45A (Bruker–AXS, 2003). Data were corrected using empirical absorption correction (SADABS, Sheldrick, 2008). Refinement of the unit-cell parameters was based on 2404 measured reflections with $I > 10\sigma(I)$. At room temperature, the unit-cell parameters are *a* 7.5764(5), *b* 5.9507(4), *c* 8.8050(6) Å, β 112.551(2)°, *V* 366.62(4) Å^3, space group $P2_1/m$, *Z* 2. The *a*:*b*:*c* ratio is 1.2729:1:1.4800. A total of 1734 independent reflections were collected and the structure was solved and refined by means of the SHELX set of programs (Sheldrick, 2008).

DESCRIPTION OF THE STRUCTURE

Structure model

The structure was refined starting from the atom coordinates of arsenbrackebuschite (Hofmeister and Tillmanns, 1978). Site-scattering values were refined for the cation sites using two scattering curves contributing proportionally and constrained sum to full occupancy: As and V were used for the sites *T*(1) and *T*(2); Al and Fe were considered for the *M* site; Sr and Ca were used for the *A*(1) site; and Sr and Ba for the *A*(2) site. A peak of ca. 2.7 e Å^{-3} was found in the difference-Fourier map, close to the *A*(2) site (ca. 0.7 Å) and it was considered occupied by Pb. Due to the low occupancy (i.e. 0.03 a.p.f.u. of Pb) it was not added to the model. Another peak in the difference-Fourier map was found close to O(7) and added to the model as an H atom with fixed coordinates and isotropic displacement factor of 0.02 Å^2 and full occupancy. Scattering curves for neutral atoms were taken from International Tables for Crystallography (Wilson, 1992). Refinement converged to $R_1 = 0.029$ for 1442 observed reflections with $F_o > 4\sigma(F_o)$ and 84 parameters. Tables 4, 5 and 6 report, respectively, atom coordinates, displacement parameters, and selected bond distances and angles. Bond valence calculations using the parameters of Brown (1981) are reported in Table 7.

Tables of structure factors and a CIF have been deposited with the Principal Editor of Mineralogical Magazine and are available from www.minersoc.org/pages/e_journals/dep_mat_mm.html.

Site occupancies

Cation sites

The observed site scattering 15.40(3) e.p.s. (electrons per site) at the *M* site agrees well with the chemical data confirming an Al dominance at that site ($Al_{0.68}$ + $Mg_{0.13}$ = 0.81 from chemical analysis, to be compared with 0.82 Al a.p.f.u., atoms per formula unit, from the refinement), with a minor contribution of heavier scatterers ($Fe^{3+}_{0.14}Mn^{3+}_{0.12}$ = 0.26 a.p.f.u. versus 0.18 Fe a.p.f.u. from the refinement, Table 4). The observed average bond length at *M* sites (1.962 Å, Table 6) is too short for Fe^{2+} and Mn^{2+}. In addition, incident bond valence at the *M* site is in agreement with average charge being dominantly 3+, i.e. considering both Fe^{3+} and Mn^{3+} at the *M* sites. The trivalent oxidation state of Fe and Mn agrees with the oxidized nature of the ore. Therefore, both elements were considered in trivalent oxidation state for formula calculation (see chemistry above). Site distribution at the *A* sites was obtained according to the structure refinement that shows a clear difference in scattering in both sites: 29.9(1) electrons per site at the *A*(1) site, and 39.4(2) electrons per site at the *A*(2). Therefore, we assign $Sr_{0.55}Ca_{0.45}$ to A(1) and $Sr_{0.92}Ba_{0.08}$ to A(2). Bond valence calculations indicate that both *A*(1) and *A*(2) sites are compatible with the dominance of divalent cations at these sites. Site scattering values obtained for *T* sites are equal, although average bond lengths and distortion parameters were significantly different (Table 6). The limited quantity of V observed in WDS analyses and the absence of high-charge cations that may potentially enter the *T* sites (P, S, Si) lead us to consider V disordered equally among both sites. The distortion is therefore interpreted an intrinsic feature of the structure. The cation sums at *T* sites implies $T^{5+}_4M^{3+}_2A^{2+}_4$ which accounts for 34^+.

Anion sites

317 There are 7 anion positions in the structure of grandaite, two of them on general position,
318 accounting for a total of 18 anions per unit cell. Bond valence table (Table 7) shows that one out of
319 7 anions sites show bond valence incidence close to 2 vu (valence units), while O(7) site has a
320 lower contribution (1.272 vu) compatible with a monovalent anion at this site. The absence of
321 fluorine in the chemical analyses (Table 2) indicates that this site must therefore host an hydroxyl
322 group. In fact, a maxima was found at ca. 0.96 Å in the Fourier difference and added to the model
323 as atom H(7). The hydrogen at H(7) is at 1.895 Å from the O(5) atom which has a bond-valence
324 sum of 1.55 vu, and so is likely to receive a hydrogen bond. Therefore there is a hydrogen bond
325 with oxygen at O(5) ensuring a further contribution of bond valence to this site (Table 7). The
326 structural model thus confirms O–H···O = 2.8 Å, in good agreement with IR data. The anion part of
327 the structure is $O_{16}(OH)_2$, which accounts for 34^-.
328
329 **Structure topology**
330 The crystal structure of grandaite (Fig. 5-6) is topologically identical to that of
331 arsenbrackebuschite. Chains of $[M^{3+,2+}(T^{5+}O_4)_2(OH, H_2O)]$ units are connected through interstitial
332 divalent cations. The M^{3+} octahedron shares edges with other octahedra forming a chain along
333 [010]. The shared edge has one anion that can be an OH group or a H_2O molecule, depending on the
334 charge of the cation at the octahedron, and the other anion is shared with the apex of a $T^{5+}O_4$
335 tetrahedron (the *T*(1) site). The remaining 4 anions coordinating the octahedron are linked to the
336 edge of another $T^{5+}O_4$ tetrahedron (the *T*(2) site) alternating in both sides (Figure 6). Minor
337 vanadium is disordered among the two arsenate tetrahedra. Decorated chains of octahedra link
338 together through bonding with two symmetrically independent interstitial cations at the *A*(1) and
339 *A*(2) sites, and hydrogen bonding (O···O = 2.8 Å). Minor Ca orders preferentially in the smaller
340 eight–coordinated *A*(1) site (<*A*(1)–O> = 2.634 Å), while minor Ba orders in the larger
341 eleven–coordinated *A*(2) site (<*A*(2)–O> = 2.811 Å) in grandaite. In arsenbrackebuschite Pb

occupies both sites but is shifted off-center as usual for its lone pair configuration. The small quantity of lead found in grandaite at the *A*(2') site follows also this configuration. This Pb off-center displacement has been previously reported; e.g., synthetic $Pb_2(Pb,K)_4[Si_8O_{20}]O$ (Moore *et al*., 1985), Pb replacing Ba in hyalotekite (Moore *et al*., 1982; Christy *et al*., 1998), or Pb replacing REE in lusernaite-(Y) (Biagioni *et al*., 2013). The distortion observed for the *T*(2) site, along with the low bond valence incidence at O(5) represents a stressed environment for this structure.

RELATED MINERALS

Grandaite, $Sr_2Al(AsO_4)_2(OH)$, is the As–dominant analogue of goedkenite, $Sr_2Al(PO_4)_2(OH)$, and the Sr–As–dominant analogue of bearthite, $Ca_2Al(PO_4)_2(OH)$. It is the first Al member of the arsenbrackebuschite group in the brackebuschite supergroup (Table 8). The brackebuschite supergroup has general formula $^{viii,xi}A_2^{2+,1+}\ ^{vi}M^{3+,2+}\ H_{0-1}\ [^{iv}(T^{5+,6+})O_4]_2\ [O_y,(OH)_{1-y}]$. Subgroups are divided on the basis of the charge species dominance at the *T* sites. The crystal chemistry of this supergroup is under study as part of a broader project. We have reported a comparison of the properties of the members of the arsenbrackebuschite group in Table 9. In the Strunz System (Strunz and Nickel, 2001) grandaite fits in subdivision 8.B.G, phosphates, *etc*. with additional anions, without H_2O, with medium-sized and large cations, (OH, *etc*.).

Isotypic structures occur in the synthetic compounds $Na_2Cr^{3+}(Cr^{6+}O_4)_2(OH)$, $K_2Cr^{3+}(Cr^{6+}O_4)_2(OH)$ (Jonsson, 1970) and $Pb_3(P_{1.15}V_{0.85})_2O_8$ (Kiat *et al*., 1993). The minerals fornacite, $Pb_2Cu^{2+}[(CrO_4)(AsO_4)](OH)$ (Lacroix, 1915, 1916; Cocco *et al*., 1967; Fanfani and Zanazzi, 1968) and vauquelinite, $Pb_2Cu^{2+}[(CrO_4)(PO_4)](OH)$ (Berzelius, 1818; Fanfani and Zanazzi, 1968), the members of the törnebohmite group [törnebohmite-(Ce), $Ce_2Al(SiO_4)_2(OH)$, and törnebohmite-(La), $La_2Al(SiO_4)_2(OH)$ (Geijer, 1921; Wherry, 1921; Shen and Moore, 1982)], molybdofornacite, $Pb_2Cu^{2+}[(MoO_4)(AsO_4)](OH)]$ (Medenbach *et al*., 1983), and the potential, but never approved, P-analogue of molybdofornacite, $[Pb_2Cu^{2+}[(MoO_4)(PO_4)](OH)$, (Nickel and Hitchen, 1994)] present derivative structure analogues characterized by doubling of one unit cell

parameter or a shift in the origin (and different symmetry). These structures are topologically identical to brackebuschite supergroup structures, the doubling of the cell being due to ordering of anions in the structure of fornacite and the shift of the origin and different symmetry elements due to order of Cu at the *M* sites in vauquelinite, probably due to Jahn–Teller effects. The latter are also structurally related to the members of descloizite, fairfieldite, roselite and tsumcorite groups.

ACKNOWLEDGMENTS

Authors wish to thank Bruno Lombardo (CNR-IGG- Torino) for his assessment support in field work at the Valletta, and Fabio Bellatreccia (Università di Roma Tre) for providing IR data. FC acknowledges Chiara Domeneghetti (Università di Pavia) for access to the Bruker-AXS diffractometer under a collaboration agreement between the Dipartimento di Scienze della Terra (Università di Torino) and the Dipartimento di Scienze della Terra e Ambiente (Università di Pavia). . Carmelo Sibio (Università di Torino) is thanked for his skill on thin section preparation. Raul Carampin (CNR-IGG-Padova, Italy) is thanked for his support on the WDS analysis. Cristian Biagioni, Mark Welch and Pete Leverett are thanked for their constructive reviews. FC, PB and EC thank the support of the project "PROactive Management of GEOlogical Heritage in the PIEMONTE Region" (www.progeopiemonte.it/en) co-founded by the University of Turin – Compagnia di San Paolo Bank Foundation "JCAPC - Progetti di Ateneo 2011" grant on line B1 "Experimental Sciences and Technology" (Project Id: ORTO11Y7HR, P.I. Prof. Marco Giardino). . FC and EB thank the MIUR and the AMI for the co-funding of a research contract for EB for the year 2013

REFERENCES

Abraham, K., Kautz, K., Tillmanns, E. and Walenta, K. (1978) Arsenbrackebuschite, $Pb_2(Fe,Zn)(OH,H_2O)[AsO_4]_2$, a new arsenate mineral. *Neues Jahrbuch für Mineralogie, Monatshefte*, 193–196.

Antofilli, M., Borgo, E. and Palenzona, A. (1983) *I nostri minerali. Geologia e mineralogia in Liguria*, 296 p. SAGEP Editrice, Genova (in Italian).

Basso, R., Palenzona, A. and Zefiro, L. (1987) Gamagarite: new occurrence and crystal structure refinement. *Neues Jahrbuch für Mineralogie, Monatshefte*, 295–304.

Biagioni, C., Bonaccorsi, E., Cámara, F., Cadoni, M., Ciriotti, M.E., Bersani, D. and Kolitsch, U. (2013) Lusernaite-(Y), $Y_4Al(CO_3)_2(OH,F)_{11}\cdot 6H_2O$, a new mineral species from Luserna Valley, Piedmont, Italy: Description and crystal structure. *American Mineralogist*, **98**,1322-1329.

Berzelius, J. (1818) Undersökning af ett hittills obemärkt Fossil, som stundom följer den Siberiska kromsyrade blyoxiden. *Afhandlingar i Fysik, Kemi och Mineralogi*, **6**, 246–254 (in Swedish).

Bideaux, R.A., Nichols, M.C. and Williams, S.A. (1966) The arsenate analog of tsumebite, a new mineral. *American Mineralogist*, **51**, 258–259.

Borgo, E. and Palenzona, A. (1988) *I nostri minerali. Geologia e mineralogia in Liguria. Aggiornamento* 1988, 48 p. SAGEP Editrice, Genova (in Italian).

Brown, I.D. (1981) The bond-valence method: an empirical approach to chemical structure and bonding. Pp. 1–30. *Structure and Bonding in Crystals* II, (M. O'Keeffe and A. Navrotsky, editors), Academic Press, New York.

Brugger, J. and Gieré, R. (1999) As, Sb, and Ce enrichment in minerals from a metamorphosed Fe-Mn deposit (Val Ferrera, Eastern Swiss Alps). *The Canadian Mineralogist*, **37**, 37–52.

Bruker–AXS (2003) SAINT. Data Reduction Software, version 6.45A Wisconsin, USA.

Brunet, F. and Chopin, C. (1995) Bearthite, $Ca_2Al(PO_4)_2OH$: stability, thermodynamic properties and phase relations. *Contributions to Mineralogy and Petrology*, **121**, 258–266.

Busz, K. (1912) Tsumebit, ein neues Mineral von Otavi und Zinnsteinkristalle. *Deutschen Naturforscher und Artze in Münster*, **84**, 230–230 (in German).

418 Chopin, C., Brunet, F., Gebert, W., Medenbach, O. and Tillmanns, E. (1993) Bearthite,
419 $Ca_2Al[PO_4]_2(OH)$, a new mineral from high-pressure terranes of the western Alps.
420 *Schweizerische Mineralogische und Petrographische Mitteilungen*, **73**, 1–9.
421 Clark, A.M., Criddle, A.J., Roberts, A.C., Bonardi, M. and Moffatt, E.A. (1997) Feinglosite, a new
422 mineral related to brackebuschite, from Tsumeb, Namibia. *Mineralogical Magazine*, **61**, 285–
423 289.
424 Christy, A.G., Grew, E.S., Mayo, S.C., Yates, M.G. and Belakovskiy, D.I. (1998) Hyalotekite,
425 $(Ba,Pb,K)_4(Ca,Y)_2Si_8(B,Be)_2(Si,B)_2O_{28}F$, a tectosilicate related to scapolite: new structure
426 refinement, phase transitions and a short-range ordered 3b superstructure. *Mineralogical*
427 *Magazine*, **62**, 77–92.
428 Cocco, G., Fanfani, L. and Zanazzi, P.F. (1967) The crystal structure of fornacite. *Zeitschrift für*
429 *Kristallographie*, **124**, 385–397.
430 De Villiers, J.E. (1943) Gamagarite, a new vanadium mineral from the Postmasburg manganese
431 deposits. *American Mineralogist*, **28**, 329–335.
432 Donaldson, D.M. and Barnes, W.H. (1955) The structures of the minerals of the descloizite group
433 and adelite groups: III – brackebuschite. *American Mineralogist*, **40**, 597-613.
434 Emsley, J. (2011) Arsenic. P. 47–55. *Nature's Building Blocks: An A-Z Guide to the Elements*,
435 Oxford University Press, Oxford, England.
436 Fanfani, L. and Zanazzi, P.F. (1967) Structural similarities of some secondary lead minerals.
437 *Mineralogical Magazine*, **36**, 522–529.
438 Fanfani, L. and Zanazzi, P.F. (1968) The crystal structure of vauquelinite and the relationships to
439 fornacite. *Zeitschrift für Kristallographie*, **126**, 433–443.
440 Foley, J.A., Hughes, J.M. and Lange, D. (1997) The atomic arrangement of brackebuschite,
441 redefined as $Pb_2(Mn^{3+},Fe^{3+})(VO_4)_2(OH)$, and comments on Mn^{3+} octahedra. *The Canadian*
442 *Mineralogist*, **35**, 1027–1033.

443 Franchi, S. and Stella, A. (1930*) Carta Geologica d'Italia 1:100.000: Foglio 78-79* (Argentera-
444 Dronero). 1ª edizione. Regio Ufficio Geologico. Stabilimento Tipografico L. Salomone, Roma
445 (in Italian).
446 Frost, R.L. and Keeffe, E.C. (2011) The mixed anion mineral parnauite
447 $Cu_9[(OH)_{10}|SO_4|(AsO_4)_2]\cdot 7H_2O$ – A Raman spectroscopic study. *Spectrochimica Acta Part A*,
448 **81**, 111–116.
449 Geijer, P. (1921) The cerium minerals of Bastnäs at Riddarhyttan. *Sveriges Geologiska*
450 *Undersökning Årsbok*, **14**(6), 3–24.
451 Gidon, M., Kerchove, C., Michard, A., Tricart, P. and Goffé, B. (1994) *Carte Géologique de la*
452 *France à 1:50.000. Feuille Aiguille de Chambeyron (872)*. Notice Explicative. BRGM, Service
453 Géologique National, Orléans (in French).
454 González del Tánago, J., La Iglesia, Á., Rius, J. and Fernández Santín, S. (2003) Calderónite, a new
455 lead-iron-vanadate of the brackebuschite group. *American Mineralogist*, **88**, 1703–1708.
456 Hak, J., Johan, Z., Kvaček, M. and Liebscher, W. (1969) Kemmlitzite, a new mineral of the
457 woodhouseite group. *Neues Jahrbuch für Mineralogie, Monatshefte*, **1969**, 201–212.
458 Harlow, G.E., Dunn, P.J. and Rossman, G.R. (1984) Gamagarite: a re-examination and comparison
459 with brackebuschite-like minerals. *American Mineralogist*, **69**, 803–806.
460 Hofmeister, W. and Tillmanns, E. (1978) Strukturelle untersuchungen an arsenbrackebuschit.
461 *Tschermaks Mineralogische und Petrographische Mitteilungen*, **25**, 153–163 (in German).
462 Horiba Jobin Yvon GmbH (2004, 2005) LabSpec [Software for Raman spectroscopic data analysis,
463 acquisition and manipulation]. Version 5.64.15.
464 Jonsson, O. (1970) The crystal structure of $Na_2Cr_3O_8OH$ and $K_2Cr_3O_8OH$. *Acta Chemica*
465 *Scandinavica*, **24**, 3627–3644.
466 Kiat, J.M., Garnier, P., Calvarin, G. and Pinot, M. (1993) Structural study of lead
467 orthophosphovanadates: role of the electron lone pairs in the phase transitions. *Journal of Solid*
468 *State Chemistry*, **103**, 490–503.

Lacroix, A. (1915) Note préliminaire sur une nouvelle espèce minérale (furnacite), provenant du Moyen Congo (Afrique équatoriale française). *Bulletin de la Société française de Minéralogie*, **38**, 198–200 (in French).

Lacroix, A. (1916) Erratum concernant une nouvelle espèce minérale du Congo. *Bulletin de la Société française de Minéralogie*, **39**, 84–84 (in French).

LaForge, L. (1938) Crystallography of tsumebite. *American Mineralogist*, **23**, 772–782.

Larson, A.C. and Von Dreele, R.B. (1994) General Structure Analysis System (GSAS). Los Alamos National Laboratory Report LAUR, 86–748.

Lefèvre, R. (1982) *Les nappes briançonnaises internes et ultra-briançonnaises dans les Alpes Cottiennes méridionales*. Thèse Scientifique, Université Paris Sud - Paris XI, Orsay (in French).

Libowitzky, E. (1999) Correlation of O-H stretching frequencies and O-H···O hydrogen bond lengths in minerals. *Monatshefte für Chemie*, **130**, 1047–1059

Mandarino, J.A. (1979) The Gladstone-Dale relationship. Part III. Some general applications. *The Canadian Mineralogist*, **17**, 71–76.

Mandarino, J.A. (1981) The Gladstone-Dale retationship. Part IV. The compatibility concept and its application. *The Canadian Mineralogist*, **19**, 441–450.

Mangione, T.G. (1999) Allume, vetriolo, ferro: attività minerarie e metallurgiche nel marchesato di Saluzzo (secoli XIV-XVI). Pp. 79–101. *Miniere, fucine, metallurgia nel Piemonte medievale e moderno*. (R. Comba, editor). Società per gli Studi Storici Archeologici e Artistici della Provincia di Cuneo, Centro studi storico-etnografici, Museo provinciale "Augusto Doro", Rocca de' Baldi, Cuneo (in Italian).

Matsubara, S., Miyawaki, R., Yokoyama, K., Shimizu, M. and Imai, H. (2004) Tokyoite, $Ba_2Mn^{3+}(VO_4)_2(OH)$, a new mineral from the Shiromaru mine, Okutama, Tokyo, Japan. *Journal of Mineralogical and Petrological Sciences*, **99**, 363–367.

494 Medenbach, O., Abraham, K. and Gebert, W. (1983) Molybdofornacit, ein neues Blei–Kupfer–
495 Arsenat–Molybdat–Hydroxid von Tsumeb, Namibia. *Neues Jahrbuch für Mineralogie,*
496 *Monatshefte*, 289–295 (in German).
497 Momma, K. and Izumi, F. (2011) VESTA 3 for three-dimensional visualization of crystal,
498 volumetric and morphology data. *Journal of Applied Crystallography*, **44**, 1272–1276.
499 Moore, P.B., Irving, A.J. and Kampf, A.R. (1975) Foggite, $CaAl(OH)_2(H_2O)[PO_4]$; goedkenite,
500 $(Sr,Ca)_2Al(OH)[PO_4]_2$; and samuelsonite $(Ca,Ba)Fe^{2+}{}_2Mn^{2+}{}_2Ca_8Al_2(OH)_2[PO_4]_{10}$: three new
501 species from the Palermo No. 1 Pegmatite, North Groton, New Hampshire. *American*
502 *Mineralogist*, **60**, 957–964.
503 Moore, P.B., Araki, T. and Ghose, S. (1982) Hyalotekite, a complex lead borosilicate: Its crystal
504 structure and the lone-pair effect of Pb(II). *American Mineralogist*, **67**, 1012–1020.
505 Moore, P.B., Sen Gupta, P.K., and Schlemper, E.O. (1985) Solid solution in plumbous potassium
506 oxysilicate affected by interaction of a lone pair with bond pairs. *Nature*, **318**, 548–550.
507 Mukherjee, A., Sengupta, M.K. and Hossain, M.A. (2006) Arsenic contamination in groundwater:
508 A global perspective with emphasis on the Asian scenario. *Journal of Health Population and*
509 *Nutrition*, **24**(2), 142–163.
510 Myneni, S.C.B., Traina, S.J., Waychunas, G.A. and Logan, T.J. (1998a) Experimental and
511 theoretical vibrational spectroscopic evaluation of arsenate coordination in aqueous solutions
512 and solids. *Geochimica et Cosmochimica Acta*, **62**, 3285–3300.
513 Myneni, S.C.B., Traina, S.J., Waychunas, G.A. and Logan, T.J. (1998b) Vibrational spectroscopy
514 of functional group chemistry and arsenate coordination in ettringite. *Geochimica et*
515 *Cosmochimica Acta*, **62**, 3499–3514.
516 Nakamoto, K. (1986) *Infrared and Raman Spectra of Inorganic and Coordination Compounds*.
517 Wiley, New York.
518 Nickel, E.H. and Hitchen, G. (1994) The phosphate analog of molybdofornacite from Whim Creek,
519 Western Australia. *Mineralogical Record*, **25**, 203–204.

Nichols, M.C. (1966) The structure of tsumebite. *American Mineralogist*, **51**, 267–267.

Norman, N.C. (editor) (1998) *Chemistry of arsenic, antimony and bismuth*, 483 p. Blackie Academic and Professional, London.

Palenzona, A. (1991) *I nostri minerali. Geologia e mineralogia in Liguria. Aggiornamento 1990*, p. 48. Amici Mineralogisti Fiorentini, Associazione Piemontese Mineralogia Paleontologia & Mostra Torinese Minerali, Centro Mineralogico Varesino, Gruppo Mineralogico "A. Negro" Coop Liguria (GE), Gruppo Mineralogico Lombardo, Gruppo Mineralogico Paleontologico "3M" Ferraia (Savona), (in Italian).

Palenzona, A. (1996) I nostri minerali. Geologia e mineralogia in Liguria, Aggiornamento 1995. *Rivista Mineralogica Italiana*, **2**, 149–172 (in Italian).

Pekov, I.V. (2007) New minerals from former Soviet Union countries, 1998-2006: new minerals approved by the IMA Commission on New Minerals and Mineral Names. *Mineralogical Almanac*, **11**, 9–51.

Pekov, I.V., Kleimenov, D.A., Chukanov, N.V., Yakubovich, O.V., Massa, W., Belakovskiy, D.I. and Pautov, L.A. (2002) Bushmakinite $Pb_2Al(PO_4)(VO_4)(OH)$, a new mineral of the brackebuschite group from oxidized zone of Berezovskoye gold deposit, the Middle Urals. *Zapiski Vserossijskogo Mineralogicheskogo Obshchestva*, **131**, 62–71.

Piccoli, G.C. (editor) (2002) *Minerali delle Alpi Marittime e Cozie Provincia di Cuneo*, p. 147–148. Amici del Museo "F. Eusebio", Alba, Cuneo, Italy (in Italian).

Pipino, G. (2010) *Documenti minerari degli stati sabaudi*, 323 p. Museo Storico dell'Oro Italiano, Tipografia Pesce, Ovada (Alessandria) (in Italian).

Pouchou, J.L. and Pichoir, F. (1984) A new model for quantitative analysis: Part I. Application to the analysis of homogeneous samples. *La Recherche Aerospatiale*, **3**, 13–38.

Pouchou, J.L. and Pichoir, F. (1985) `PAP' φ(ρZ) procedure for improved quantitative microanalysis. Pp. 104–106. *Microbeam Analysis* (J.T. Armstrong, editor). San Francisco Press, San Francisco, California, USA.

546 Rammelsberg, C. (1880) Über die vanadinerze aus dem Staat Córdoba in Argentinien. *Zeitschrift*
547 *der Deutschen Geologischen Gesellschaft*, **32**, 708–713 (in German)
548 Robinson, K., Gibbs, G.V. and Ribbe, P.H. (1971) Quadratic elongation: a quantitative measure of
549 distortion in coordination polyhedra. *Science*, **172**, 567–570.
550 Rosický, V. (1912) Preslit, ein neues Mineral von Tsumeb in Deutsch-Südwestafrika. *Zeitschrift für*
551 *Krystallographie und Mineralogie*, **51**, 521–526 (in German).
552 Roth, P. (2007) Bearthite. In *Minerals first discovered in Switzerland and minerals named after*
553 *Swiss individuals*, pp. 44-45. Kristallografik Verlag, Achberg
554 Schlüter, J., Gebhard, G. and Wappler, G. (1994) Tsumebit oder Arsentsumebit aus Tsumeb? *Lapis*,
555 **19**(10), 31–34 (in German)
556 Sheldrick, G.M. (2008) A short history of SHELX. *Acta Crystallographica*, **A64**, 112–122.
557 Shen, J. and Moore, P.B. (1982) Törnebohmite, $RE_2Al(OH)[SiO_4]_2$: crystal structure and genealogy
558 of RE(III)Si(IV) ↔ Ca(II)P(V) isomorphisms. *American Mineralogist*, **67**, 1021–1028.
559 Spek, A.L. (2009) Structure validation in chemical crystallography. *Acta Crystallographica*, **D65**,
560 148–155.
561 Spencer, L.J. (1913) A (sixth) list of new mineral names. *Mineralogical Magazine*, **16**, 352–378.
562 Strunz, H. and Nickel, E.H. (2001) *Strunz Mineralogical Tables. Chemical Structural Mineral*
563 *Classification System*. 9th Ed., 870 p. Schweizerbart, Stuttgart.
564 Twarakavi, N.K.C and Kaluarachchi, J.J. (2006) Arsenic in the shallow ground waters of
565 conterminous United States: assessment, health risks, and costs for MCL compliance. *Journal*
566 *of American Water Resources Association*, **42**, 275–294.
567 Vaughan, D.J. (2006) Arsenic. *Elements*, **2**(2), 71–75.
568 Vésignié, J.P.L. (1935) Présentation d'échantillons. *Bulletin de la Société française de Minéralogie*,
569 **58**, 4–5 (in French).

570 Walenta, K. and Dunn, P.J. (1984) Arsenogoyazit, ein neues mineral der crandallitgruppe aus dem
571 Schwarzwald. *Schweizerische Mineralogische und Petrographische Mitteilungen*, **64**, 11–19
572 (in German).
573 Wherry, E.T. (1921) New minerals. *American Mineralogist*, **6**, 118–119.
574 Williams, S.A. (1973) Heyite, $Pb_5Fe_2(VO_4)_2O_4$, a new mineral from Nevada. *Mineralogical*
575 *Magazine*, **39**, 65–68.
576 Wilson, A.J.C. (editor) (1992) *International Tables for Crystallography. Volume C: Mathematical,*
577 *physical and chemical tables*. Kluwer Academic Publishers, Dordrecht, The Netherlands.
578 Wojdyr, M. (2010) Fityk: a general-purpose peak fitting program. *Journal of Applied*
579 *Crystallography*, **43**, 1126–1128.
580 Yakubovich, O.V., Massa, W. and Pekov, I.V. (2002) Crystal structure of the new mineral
581 bushmakinite, $Pb_2\{(Al,Cu)[PO_4][(V,Cr,P)O_4](OH)\}$. *Doklady Earth Sciences*, **382**, 100–105.
582 Zubkova, N.V., Pushcharovsky, D.Y., Giester, G., Tillmanns, E., Pekov, I.V. and Kleimenov, D.A.
583 (2002) The crystal structure of arsentsumebite, $Pb_2Cu[(As,S)O_4]_2(OH)$. *Mineralogy and*
584 *Petrology*, **75**, 79–88.
585

586
587 **TABLES**
588
589 Table 1.
590
591
592

	wt.%	Range	stand. dev.	Probe standard
SrO	29.81	28.51 – 30.57	0.64	celestine (*L*α)
CaO	7.28	6.79 – 7.74	0.48	wollastonite (*K*α)
BaO	1.56	0.79 – 2.63	0.56	baryte (*L*α)
Al_2O_3	7.07	6.76 – 7.79	0.38	Al_2O_3 (*K*α)
$Fe_2O_3^{**}$	2.34	2.09 – 2.63	0.28	Fe_2O_3 (*K*α)
Mn_2O_3	1.88	1.36 – 2.14	0.24	$MnTiO_3$ (*K*α)
MgO	1.04	0.76 – 1.40	0.18	MgO (*K*α)
PbO	0.43	0.16 – 0.55	0.13	Pb (*M*α)
As_2O_5	44.95	44.48 – 45.71	0.46	GaAs (*L*α)
V_2O_5	0.50	0.32 – 0.65	0.12	vanadinite (*K*α)
P_2O_5	0.09	0.06 – 0.12	0.02	apatite (*K*α)
H_2O^*	1.83	1.82 – 1.86	0.01	
Total	98.78	98.23 – 99.18	0.30	

Notes: *Calculated by stoichiometry from the results of the crystal structure analysis; **All Fe is considered as Fe^{3+} on the basis of structure refinement results.

593
594
595 Table 1. Analytical data for grandaite
596

597
598 Table 2.
599

h	*k*	*l*	d_{obs} (Å)	d_{calc} (Å)	I_{rel}	I_{calc}
0	0	1		8.131		10.9
0	0	2		4.066		9.3
1	1	1		3.597		11.7
2	0	0		3.499		12.5
0	1	2		3.357		6.3
-2	**1**	**1**	**3.194**	**3.193**	**100.00**	**100.0**
0	**2**	**0**	**2.981**	**2.975**	**50.93**	**83.0**
-1	**0**	**3**	**2.922**	**2.935**	**40.20**	**80.4**
-2	1	2		2.930		11.6
2	0	1		2.842		14.2
0	2	1	2.798	2.794	6.55	8.2
1	**2**	**0**	**2.743**		**31.39**	
1	**1**	**2**	**2.705**	**2.710**	**65.19**	**61.0**
2	1	1	2.563	2.565	5.02	9.7
1	2	1	2.486	2.485	21.13	10.8
-2	1	3	2.455	2.461	16.05	9.3
0	2	2	2.400		7.45	
-3	1	1	2.315		12.81	
3	0	0		2.332		7.2
-2	0	4	2.144	2.153	8.04	11.9
1	2	2	2.127		11.19	
2	1	2	2.108		5.38	
-1	**2**	**3**	**2.087**	**2.089**	**51.75**	**29.5**
-1	1	4	2.047		7.05	
3	0	1		2.044		18.0
-2	1	4	2.017		5.55	
-2	2	3	1.999		5.56	
-4	0	2	1.891	1.892	10.70	22.8
-3	1	4	1.845	1.850	22.42	16.5
-4	0	3		1.822		8.9
-2	3	1	1.759		10.32	
-2	3	1		1.757		13.1
2	1	3	1.745		5.93	
4	0	0		1.749		6.0
3	**2**	**1**	**1.685**	**1.685**	**24.52**	**19.9**
1	**3**	**2**	**1.663**	**1.662**	**27.65**	**13.1**
-4	2	2	1.597	1.596	14.40	9.8

Notes: *Only reflections with $I_{rel} > 5\sigma(I_{rel})$ are listed.

600
601
602 Table 2. X–ray powder diffraction data for grandaite. The eight
603 strongest reflections are reported in bold *

Table 3.

Crystal system	Monoclinic
Space group	$P2_1/m$
Unit–cell dimensions	
a (Å)	7.5764(5)
b (Å)	5.9507(4)
c (Å)	8.8050(6)
β (°)	112.551(2)
V (Å^3)	366.62(4)
Z	2
μ (mm^{-1})	20.34
F(000)	443
D_{calc} (g cm^{-3})	4.378
Crystal size (mm)	0.130 × 0.085 × 0.080
Radiation type	Mo $K\alpha$ (0.71073 Å)
Temperature (K)	298
θ–range for data collection (º)	2.5-35.0
R_{int}	0.026
Reflections collected	6095
Independent reflections	1734
F_o>4σ(F)	1442
Refinement method	least-squares matrix: full
No. of refined parameters	84
Final R_{obs}	0.037
R_1	0.029
wR_2 F_o>4σ(F)	0.065
Highest peak/deepest hole (e Å^{-3})	+2.57 / -0.76
Goodness of fit on F^2	1.074

Table 3. Crystal data and summary of parameters describing data collection and refinement for grandaite

635

636 Table 4.

637

Site	Mult.	Occ.	*x*/*a*	*y*/*b*	*z*/*c*	U_{iso}
T(1)	2*e*	0.886(9)As 0.114(9)V	0.43733(5)	1/4	0.17111(4)	0.0124(1)
T(2)	2*e*	0.884(9)As 0.116(9)V	0.03113(4)	1/4	0.33393(4)	0.0103(1)
M	2*a*	0.815(5)Al 0.185(5)Fe	0	0	0	0.0106(2)
A(1)	2*e*	0.548(5)Sr 0.452(5)Ca	0.25931(6)	1/4	0.73723(5)	0.0188(1)
A(2)	2*e*	0.921(7)Sr 0.079(7)Ba	0.67546(4)	1/4	0.58860(4)	0.0133(1)
O(1)	4*f*		0.0231(3)	0.5144(3)	0.7853(2)	0.0203(4)
O(2)	2*e*		0.2635(4)	1/4	0.4501(3)	0.0265(6)
O(3)	2*e*		0.9109(4)	1/4	0.4550(4)	0.0320(7)
O(4)	4*f*		0.5055(2)	0.0223(3)	0.2905(2)	0.0197(4)
O(5)	2*e*		0.5209(5)	1/4	0.0207(4)	0.0391(8)
O(6)	2*e*		0.1923(3)	1/4	0.0638(3)	0.0210(5)
O(7)	2*e*		0.8303(3)	1/4	0.9207(3)	0.0137(5)
H(7)	2*e*	1.000	0.7043	1/4	0.9230	0.0200

Notes: *The temperature factor has the form exp(-T) where $T = 8\pi^2 U(\sin(\theta)/\lambda)^2$ for isotropic atoms.

638

639 Table 4. Multiplicities, fractional atom coordinates, and equivalent isotropic displacement
640 parameters ($Å^2$) for grandaite*

641

642

643 Table 5.
644
645

site	U_{11}	U_{22}	U_{33}	U_{23}	U_{13}	U_{12}
T(1)	0.0124(2)	0.0114(2)	0.0114(2)	0	0.00242(12)	0
T(2)	0.0124(2)	0.0105(2)	0.0093(2)	0	0.00556(12)	0
M	0.0139(4)	0.0087(4)	0.0090(4)	0.0000(2)	0.0039(3)	-0.0004(2)
A(1)	0.0179(2)	0.0206(2)	0.0226(2)	0	0.0131(2)	0
A(2)	0.0147(2)	0.01477(14)	0.01246(15)	0	0.00758(10)	0
O(1)	0.0330(1)	0.0132(7)	0.0156(8)	0.0020(6)	0.0105(7)	0.0025(6)
O(2)	0.0152(12)	0.040(2)	0.0217(13)	0	0.0041(10)	0
O(3)	0.0334(15)	0.041(2)	0.035(2)	0	0.0273(14)	0
O(4)	0.0226(8)	0.0153(8)	0.0177(8)	0.0026(6)	0.0039(7)	0.0017(6)
O(5)	0.041(2)	0.059(2)	0.028(2)	0	0.0249(14)	0
O(6)	0.0149(11)	0.0216(12)	0.0207(12)	0	0.0005(9)	0
O(7)	0.0121(10)	0.0150(11)	0.0124(10)	0	0.0029(8)	0

Notes: *The temperature factor has the form exp(-T) where $T = 2\pi^2\Sigma_{ij}(h(i)h(j)U(i,j)a^*(i)a^*(j)$.

646
647 Table 5. Anisotropic displacement parameters ($Å^2$) for grandaite*
648
649

650 Table 6.

T(1)–O(4) (×2)	1.671(2)	*A*(1)–O(4)(×2)	2.489(2)
–O(5)	1.673(3)	–O(5)	2.523(3)
–O(6)	1.730(2)	–O(1) (×2)	2.537(2)
<*T*(1)–O>	1.686	–O(2)	2.541(3)
V(Å^3)	2.449	–O(3)	2.848(3)
σ^2*	12.93	–O(6)	3.105(3)
λ*	1.0034	<*A*(1)–O>	2.634
		V(Å^3)	26.80
T(2)–O(3)	1.647(3)		
–O(2)	1.663(3)	*A*(2)–O(3)	2.485(3)
–O(1) (×2)	1.704(2)	–O(4) (×2)	2.600(2)
<*T*(2)–O>	1.680	–O(7)	2.701(3)
V(Å^3)	2.430	–O(4) (×2)	2.791(2)
σ^2*	0.49	–O(2)	2.883(3)
λ*	1.0006	–O(1) (×2)	2.986(2)
		–O2 (×2)	3.050(1)
M–O(7) (×2)	1.914(1)	<*A*(2)–O>	2.811
–O(1) (×2)	1.966(2)	*V*(Å^3)	49.28
–O(6) (×2)	2.006(2)		
<*M*–O>	1.962	O(7)–H(7)	0.96
V(Å^3)	9.934	O(7)···O(5)	2.80
σ^2*	32.00	O(5)···H(7)	1.89
λ*	1.0097		

Notes: *Mean quadratic elongation (λ) and the angle variance (σ^2) were computed according to Robinson *et al*. (1971).

651

652 Table 6. Selected interatomic distances (Å) and angles (^{o}) for grandaite*

653

654 Table 7.
655
656

site	*T*(1)	*T*(2)	*M*	*A*(1)	*A*(2)	*H*(7)	Σ
O(1)		1.17 $^{\times 2\downarrow}$	0.46 $^{\times 2\downarrow}$	0.27 $^{\times 2\downarrow}$	0.10 $^{\times 2\downarrow}$		2.00
O(2)		1.30		0.27	0.13		1.88
					0.09 $^{\times 2\downarrow}$ $_{\times 2\rightarrow}$		
O(3)		1.35		0.11	0.37		1.83
O(4)	1.27 $^{\times 2\downarrow}$			0.30 $^{\times 2\downarrow}$	0.27 $^{\times 2\downarrow}$		2.01
					0.17 $^{\times 2\downarrow}$		
O(5)	1.27			0.28		0.18	1.73
O(6)	1.10		0.42 $^{\times 2\downarrow}$ $_{\times 2\rightarrow}$	0.07			2.01
O(7)			0.53 $^{\times 2\downarrow}$ $_{\times 2\rightarrow}$		0.21	0.81	2.08
b.v.	4.91	4.99	2.82	1.87	1.97	0.99	17.55
Agg. ch.	5.00	5.00	2.88	2.00	1.98	1.00	17.86

657
658
659 Table 7. Bond valence calculations for grandaite
660
661
662
663

Table 8.

Brackebuschite supergroup, $\boldsymbol{A}(1)^{2+}\boldsymbol{A}(2)^{2+}{}^{VI}[\boldsymbol{M}^{3+}_{x},\boldsymbol{M}^{2+}_{1-x}]\,[{}^{IV}(\boldsymbol{T}^{5+}_{z},\boldsymbol{T}^{6+}_{1-z})O_4]_2\,(O_{1-y}OH_y)$

Arsenbrackebuschite group As *dominant at T*	Brackebuschite group V *dominant at T*	Goedkenite group P *dominant at T*	Tsumebite group P or As + S or V *dominant at T*
Arsenbrackebuschite [1,2] $Pb_2Fe^{3+}(AsO_4)_2(OH,H_2O)$	Brackebuschite [7,8,9,10] $Pb_2Mn^{3+}(VO_4)_2(OH)$	Bearthite [17,18,19] $Ca_2Al(PO_4)_2(OH)$	Arsentsumebite [3,4,5,29] $Pb_2Cu[(AsO_4)(SO_4)](OH)$
Feinglosite [6] $Pb_2Zn(AsO_4)_2(OH,H_2O)$	Calderónite* [11] $Pb_2Fe^{3+}(VO_4)_2(OH)$	Goedkenite [23] $Sr_2Al(PO_4)_2(OH)$	Bushmakinite [20,21,22] $Pb_2Al[(PO_4)(VO_4)](OH)$
Grandaite [30] $Sr_2Al(AsO_4)_2(OH)$	Gamagarite [12,13,14] $Ba_2Fe^{3+}(VO_4)_2(OH,H_2O)$		Tsumebite [9,24,25,26,27,28,29] $Pb_2Cu[(PO_4)(SO_4)](OH)$
	Heyite* [15] $Pb_5Fe^{2+}{}_2(VO_4)_2O_4$		
	Tokyoite [16] $Ba_2Mn^{3+}(VO_4)_2(OH)$		

Refs: [1] Abraham *et al*. (1978); [2] Hofmeister and Tillmanns (1978); [3] Vésignié (1935); [4] Bideaux *et al*. (1966); [5] Zubkova *et al*. (2002); [6] Clark *et al*. (1997); [7] Rammelsberg (1880); [8] Donaldson and Barnes (1955); [9] Fanfani and Zanazzi (1967); [10] Foley *et al*. (1997); [11] González del Tánago *et al*. (2003); [12] de Villiers (1943); [13] Harlow *et al*. (1984); [14] Basso *et al*. (1987); [15] Williams (1973); [16] Matsubara *et al*. (2004); [17] Chopin *et al*. (1993); [18] Brunet and Chopin (1995); [19] Roth (2007); [20] Pekov *et al*. (2002); [21] Yakubovich *et al*. (2002); [22] Pekov (2007); [23] Moore *et al*. (1975); [24] Rosický (1912); [25] Busz (1912); [26] Spencer (1913); [27] LaForge (1938); [28] Nichols (1966); [29] Schlüter *et al*. (1994); [30] this study. *Needs further study.

Table 8. Minerals of the brackebuschite supergroup. References are given in brackets

684 Table 9.
685

	Arsenbrackebuschite	Feinglosite*	Grandaite
Reference	(1,2)	(3)	this work
Formula	$Pb_2Fe^{3+}(AsO_4)_2(OH,H_2O)$	$Pb_2Zn(AsO_4)_2{\cdot}H_2O$	$Sr_2Al(AsO_4)_2(OH)$
System	monoclinic	monoclinic	monoclinic
Space group	$P2_1/m$	$P2_1$, $P2_1/m$	$P2_1/m$
***a* (Å)**	7.764(2)	7.766(6)	7.5752(5)
b	6.045(2)	5.955(3)	5.9512(4)
c	9.022(2)	8.973(6)	8.8077(5)
β (°)	112.5	112.20(6)	112.565(1)
***V* (Å^3)**	391.2	384.2(4)	366.62(4)
Z	2	2	2
a*:*b*:*c	1.2843:1:1.4924	1.5068: 1:1.3041	1.2729:1:1.4800
D_{meas} (g cm^{-3})	n.d.	n.d.	n.d.
D_{calc} (g cm^{-3})	6.54	6.52	4.38
Strongest lines in the powder pattern: d_{obs} (Å)(I)	3.012 (100), 3.268 (90), 2.777 (60), 2.313 (30), 2.133 (30), 4.92 (25), 3.68 (25)	3.246(100), 2.988(60), 2.769 (60), 4.85(50), 2.107(50), 3.659 (30), 2.293 (30)	3.194 (100), 2.705 (65.19), 2.087 (51.75), 2.981 (50.93), 2.922 (40.20), 2.743 (31.39), 1.663 (27.65), 1.685 (24.52)
Optical (sign)	biaxial (–)	biaxial	biaxial (+)
α	n.d.	n.d.	1.726(1)
β	n.d.	n.d.	1.731(1)
γ	n.d.	n.d.	1.752(1)
2*V*(°)	n.d.	n.d.	52(2) (meas), 53 (calc)
Colour	honey-yellow, yellow, brown, green	pale olive-green	orange to salmon to brown
Pleochroism	honey-yellow to bright yellow	non pleochroic	non pleochroic
Hardness (Mohs)	4-5	4-5	6-6.5
Streak	pale brownish	white	reddish brown
Luster	resinous to adamantine	adamantine	vitreous
Fluorescent	—	—	non-fluorescent
Tenacity	—	sectile	brittle
Cleavage	perfect on {010}	—	not observed
Twinning	complex, observed	—	none observed
Habit & forms	tiny flat plates and laths	multiple individuals, in radiating botryoidal aggregates	subhedral grains
Association	beudantite, anglesite, mimetite, bayldonite, stolzite	goethite, anglesite, wulfenite, chalcocite, arsendescloizite, gypsum	aegirine, adelite, baryte, braunite, hematite, quartz, tilasite, unidentified Mn oxides and Mn silicates

Refs: [(1)] Abraham *et al*. (1978); [(2)] Hofmeister and Tillmanns (1978); [(3)] Clark *et al*. (1997); *unit cell parameters transformed to compare the structure relationships between group phases.

686
687 Table 9. Comparison of minerals of the arsenbrackebuschite group
688

689 **FIGURES**
690
691 Figure 1.

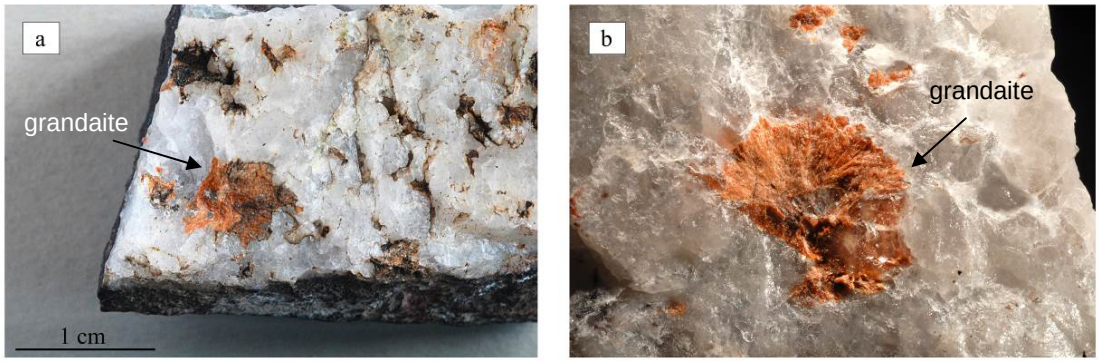

692
693

Figure 2.

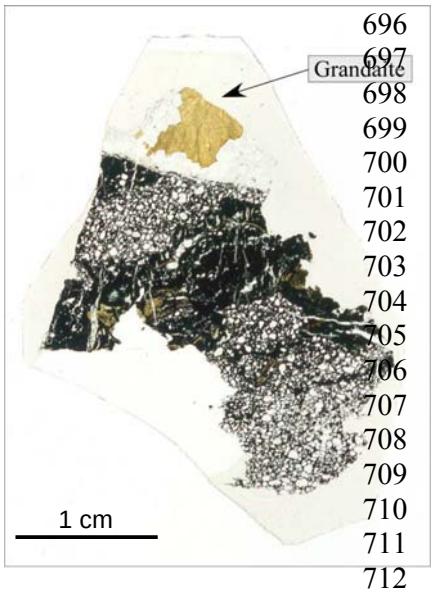

Figure 3

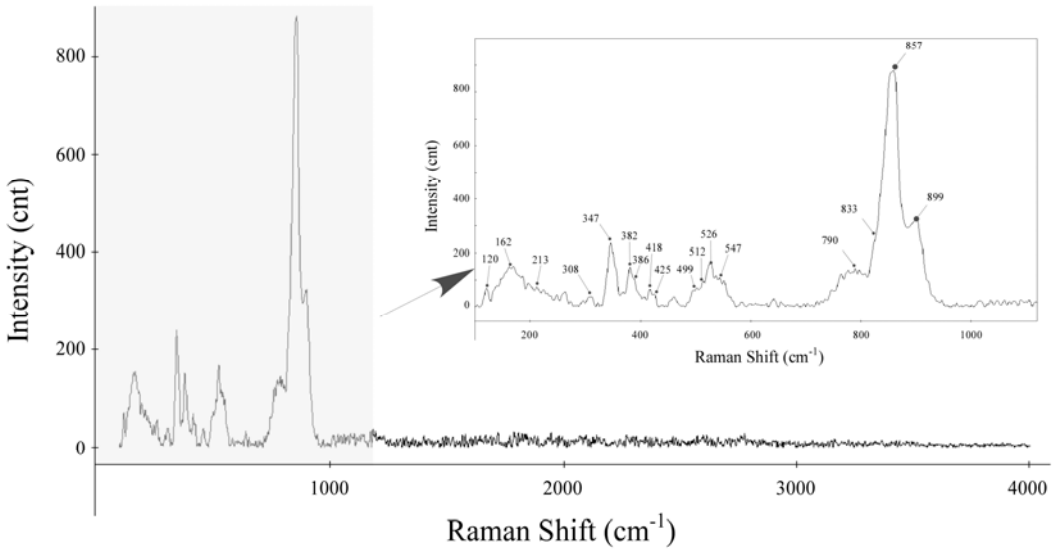
Intensity (cnt)
800
600
400
200
0
1000
2000
3000
4000
Raman Shift (cm-1)
Intensity (cnt)
800
600
400
200
0
120
162
213
308
347
382
386
418
425
499
512
526
547
790
833
857
899
200
400
600
800
1000
Raman Shift (cm-1)

Figure 4.

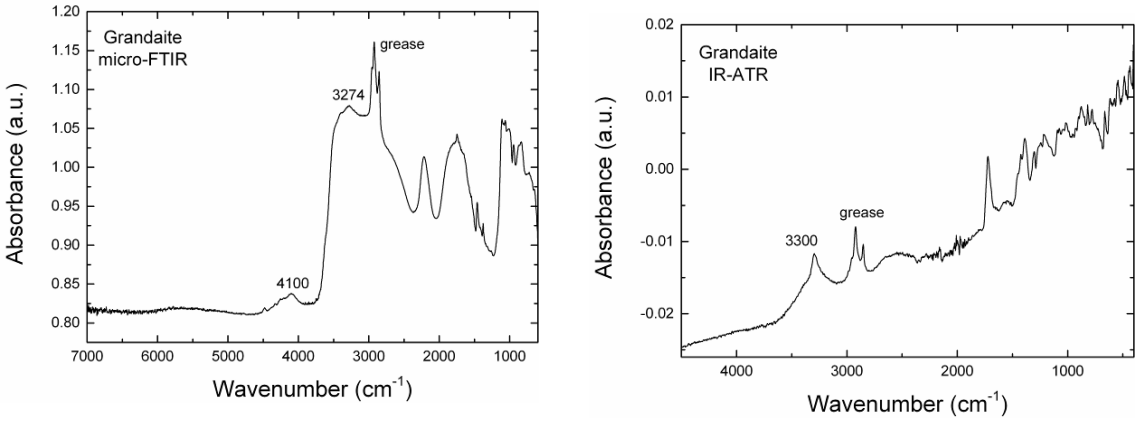
Grandaite
micro-FTIR
grease
3274
4100
Absorbance (a.u.)
Wavenumber (cm-1)
Grandaite
IR-ATR
grease
3300
Absorbance (a.u.)
Wavenumber (cm-1)

772 Figure 5.

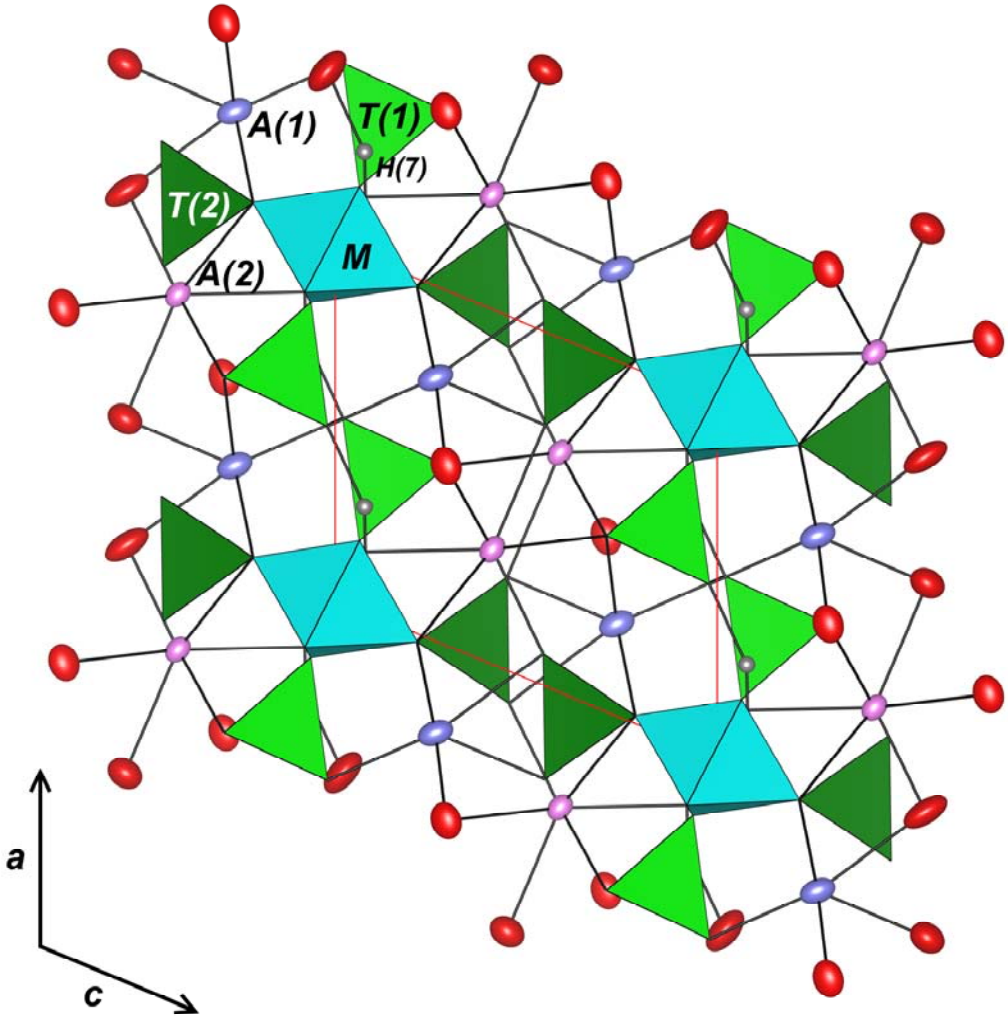

773
774
775
776

777 Figure 6.
778
779

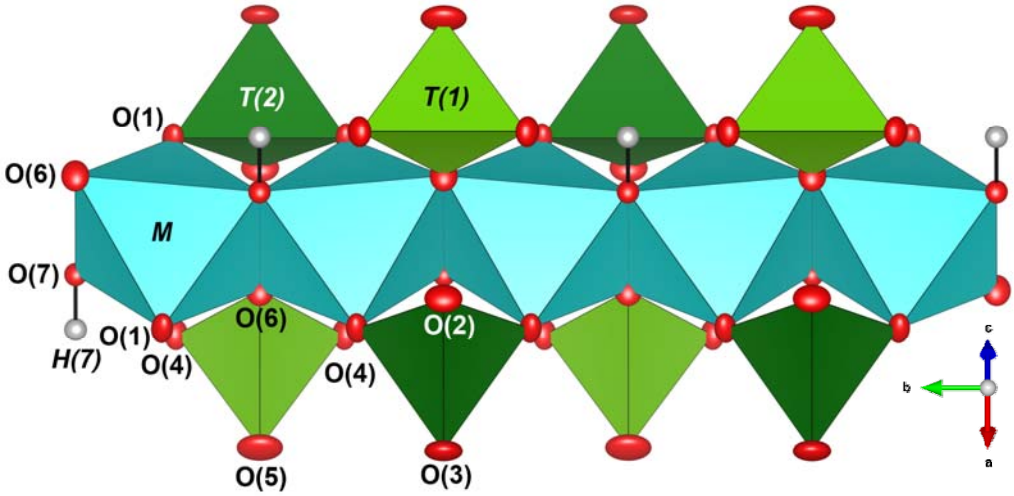

780
781
782
783

Figures captions

Figure 1. Pictures of grandaite: (a) in the holotype specimen deposited in the Museo Regionale di Scienze Naturali di Torino and (b) fan-like aggregate (~ 1 × 1 cm) of grandaite in quartz matrix, from the collection of G.C. Piccoli. Photo from G. Piccoli.

Figure 2. Image of the thin section of the holotype showing grandaite in the area marked, associated to a quartz vein, cutting a braunite-hematite-bearing quartzite. Plane-polarized light.

Figure 3. Raman spectra of grandaite in the 200-4000 cm^{-1} region and between 200 and 1200 cm^{-1}.

Figure 4. Infrared spectra: (left) single crystal infrared spectrum; (right) powder spectrum collected with a MIRacle Diamond ATR accessory.

Figure 5. Projection of the grandaite structure down [010]; the unit cell is indicated by thick red lines. Ellipsoids at 90% probability. Atom sites labelled in the figure: *T*(1) light green, *T*(2) dark green, *M* light blue, *A*(1) lilac, *A*(2) violet, *H*(7) grey, oxygen sites in red. Drawing obtained with VESTA 3 (Momma and Izumi, 2011)

Figure 6. Detail of the chain of *M*-octahedra. Ellipsoids at 50% probability. Atom sites labelled in the figure; colours as in Fig. 5. Drawing obtained with VESTA 3 (Momma and Izumi, 2011)